Robustness analysis of a parallel two-box digital polynomial predistorter for an SOA-based CO-OFDM system

C. Diouf [a], M. Younes [b], A. Noaja [c], S. Azou [a,*], M. Telescu [b], P. Morel [a], N. Tanguy [b]

[a] ENIB/CNRS UMR 6285 Lab-STICC, Brest, France
[b] Univ. de Bretagne Occidentale/CNRS UMR 6285 Lab-STICC, Brest, France
[c] Military Technical Academy, Bucharest, Romania

A B S T R A C T

The linearization performance of various digital baseband pre-distortion schemes is evaluated in this paper for a coherent optical OFDM (CO-OFDM) transmitter employing a semiconductor optical amplifier (SOA). In particular, the benefits of using a parallel two-box (PTB) behavioral model, combining a static nonlinear function with a memory polynomial (MP) model, is investigated for mitigating the system nonlinearities and compared to the memoryless and MP models. Moreover, the robustness of the predistorters under different operating conditions and system uncertainties is assessed based on a precise SOA physical model. The PTB scheme proves to be the most effective linearization technique for the considered setup, with an excellent performance-complexity tradeoff over a wide range of conditions.

1. Introduction

Orthogonal frequency-division multiplexing (OFDM) has been recognized as one of the most promising techniques to support high data rate in next-gen optical communications networks, with some important advantages like simple compensation of linear channel impairments, dynamic bandwidth allocation capability in a multiuser context, and powerful digital signal processor (DSP)-based implementation [1–3]. However, a well-known drawback of multicarrier signaling is the high Peak-to-Average-Power Ratio (PAPR) [4], which makes OFDM very sensitive to nonlinear devices. Hence, PAPR reduction has been a subject of intense research in the past decade [5], with a wide variety of approaches originally developed for wireless and wireline communications and later investigated for optical OFDM systems [6]. Recently, Amiralizadeh et al. made an important contribution to the modeling and compensation of CO-OFDM transmitter nonlinearity [7] in presence of high PAPR, with a theoretical analysis of the impact of different nonlinear components (DAC, electrical power amplifier, optical modulator) in terms of bit-error-rate (BER) for different clipping ratios. It is also proposed to apply clipping along with digital predistortion to mitigate performance degradation. Some of the present authors have investigated similar problems by considering nonlinear effects originating from optical components, with a special focus on Semiconductor Optical Amplifiers (SOAs) [8,9]. Interesting features such as low cost, large

optical bandwidth and small form factor [10] make SOAs an interesting alternative to the high-end EDFAs for some application scenarios [11]. However, as pointed out in our previous study, the use of the SOA as a booster amplifier may introduce strong nonlinear effects such as cross phase modulation (XPM) and four wave mixing (FWM) and degrade the overall system performance. PAPR reduction is required for shaping the envelope dynamics so as to limit the signal distortion but, as in [7], for a better performance improvement this may be combined with some linearization technique for compensating the nonlinear effects inherent to the SOA (which we consider as the main source of nonlinear distortion here). A broad variety of methods have been studied in literature for linearizing optical links or radio-over-fiber (RoF) links over the past few years, with a few approaches being specifically designed to cope with the nonlinear effects of SOA [12,13]. The various methods can be classified into three main groups: optical linearization, electrical analog linearization and electrical digital linearization [14]. A digital baseband predistortion (DPD) is considered throughout this study, which consists in pre-compensating the transmitter nonlinear characteristics based on a black-box behavioral model. Thus irregular characteristics of the transmitter can be counteracted in a flexible way, with a limited knowledge of physical link parameters and at a limited implementation effort. DPD has been the method of choice for power amplifier linearization in microwave wireless communication systems
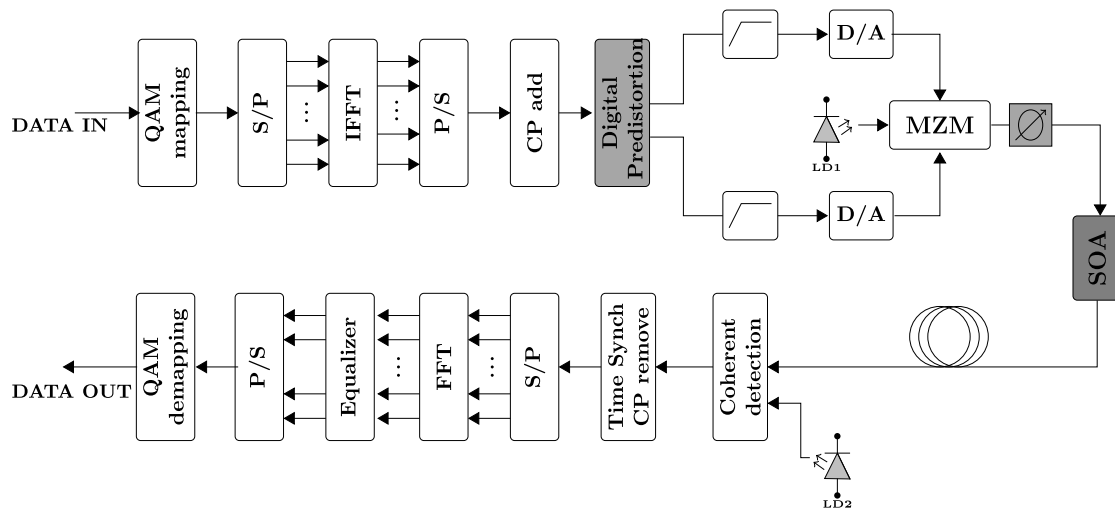
Fig. 1. CO-OFDM structure.

for a long time [15,16]. Numerous formulations exist featuring various block architectures either including or neglecting memory effects. The optical communications community has so far shown caution in importing such methods, but some proof-of-concept studies do exist and the effectiveness of DPD in optical fiber systems has been reported in a number of studies for different modulation formats (single carrier QAM, OFDM, CDMA) at various data rates and for different system setups/devices. The Memory Polynomial (MP) model [17–26], or its generalized formulation (GMP) [27,28], is extensively adopted for its good performance. The interest of using a simple look-up-table (LUT) scheme is mentioned in a few references [29–31] when the nonlinearity under test can be assumed as memoryless. It is also possible to use box-oriented models, which may be an attractive solution for lowering the implementation complexity while achieving good performance. In [32], it is proposed to combine the advantages of MP and Envelope Memory Polynomial (EMP) in a hybrid parallel structure whereas in [33] the authors study a Hammerstein model, which is composed of a memoryless nonlinearity function followed by a FIR filter. In our previous study [9], we investigated a Filter LUT scheme, which belongs to the augmented Hammerstein family, but with no special attempt to lower the complexity. The present paper tackles this issue which is crucial at optical data rates. A parallel two-box behavioral model is first examined for improving the same SOA-based transmitter, with a static nonlinear function and an MP model and with the objective of keeping the complexity as low as possible (low number of model parameters). It is proposed to design the static block by jointly considering the linearization and PAPR reduction objectives, via a simple constrained polynomial fitting. A second objective is to analyze the robustness of the predistorter in presence of parameter variations in the transmitter. Some of these parameters are physical such as the peak-to-peak voltage of the Mach–Zehnder modulator, optical power and wavelength of the optical signal or bias current for the SOA while others constitute changes in the modulation such as the number of subcarriers. To the best of the authors' knowledge this sort of analysis has not yet been conducted although it is extremely useful in the perspective of meeting future network demands, involving possibly adaptive transceiver parameters [34].

2. CO-OFDM system model

The following study is based on the coherent optical OFDM system model described in Fig. 1. The setup comprises a transmitter, a Semiconductor Optical Amplifier (SOA) device for boosting transmission reach and performance, and a receiver. Except the digital predistortion block, aiming at counteracting the SOA nonlinearities, the transmitter and receiver architectures are standard with common blocks such as QAM

mapping/demapping, serial-to-parallel (S/P)/parallel-to-serial (P/S) conversion, FFT/IFFT transforms, Cyclic Prefix (CP) adding/removing, digital-to-analog (D/A)/analog-to-digital (A/D) conversion, time synchronization and equalization. At the transmitter side electro-optical (E/O) conversion is performed by an IQ modulator (Mach–Zehnder modulator, MZM) and linked to the main transmission laser (LD1). A second laser (LD2) is used to perform the coherent detection.

To carry out analyses in interest, the setup is implemented in a Matlab-ADS co-simulation environment. The CO-OFDM transmitter and receiver are modeled in Matlab while the SOA is modeled in ADS Ptolemy using the carrier density rate and optical signal field propagation equations [8]. Optical Amplifier parameters are tuned to realistically fit a 750 μm long commercial SOA (INPHENIX-IPSAD1501). Regarding the lasers, the study assumes perfect phase noise compensation and no frequency offset on the receiver side. A standard nonlinear model of the IQ optical modulator is implemented [1], with no imbalance impairment. For the D/A and A/D, a uniform quantization is considered, with a default resolution of 12 bits throughout the manuscript; the effect of the resolution will be investigated in Section 4 by decreasing its value to 4 bits. An ideal coherent detection is assumed (ideal photodetectors).

As presented in Fig. 1, input data stream is processed by the transmitter to obtain the initial OFDM electrical signal. Hard-clipping with a threshold of 12 dB is applied on the signal in front of DACs just before E/O conversion and the signal at SOA input has its power adjusted via an optical attenuator. Then, the equivalent OFDM optical signal with the SOA model are provided to the ADS environment for simulations relying on the field propagation equations. Once the simulation has been carried out, the Amplified Spontaneous Emission (ASE) noise sequence is calculated and added to the optical signal which is finally sent in the receiver which computes output data stream (back-to-back evaluation). Throughout the paper, we consider a 17 Gbps transmission with the default parameters presented in Table 1.

The structure and identification techniques of the predistortion systems in this study will be detailed in the following section.

3. Predistortion structures

The general concept behind predistortion is to precompensate amplification impairments by distorting the signal injected to the amplifier. The operation is carried out by a predistorter which basically corresponds to an inverse function of device under study. Four polynomial-based structures will be comparatively used to model the SOA inverse function: the static predistorter, the memory polynomial predistorter, the envelope memory polynomial predistorter and the parallel twin boxes predistorter. The memoryless digital predistorter

Table 1
Transmission system parameters.

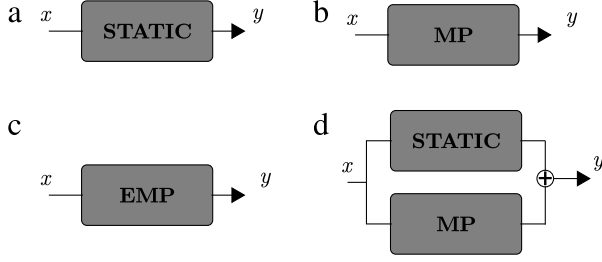|					
Bandwidth:	20 Ghz	Modulation Format:	4-QAM	Oversampling factor:	4
Sampling Time:	25.6 ns	Number of subcarriers:	512	CP length ratio:	0.125
V_{pp}:	8 Volts	Biasing current:	150 mA	Alpha factor (α_H):	3.3

Fig. 2. The four digital predistorters considered in this study: (a) Memoryless predistorter H_{ST}, (b) Memory Polynomial predistorter H_{MP}, (c) Envelope Memory Polynomial predistorter H_{EMP}, (d) Parallel twin boxes predistorter H_{PTB}.

(STATIC, Fig. 2(a)) is defined by a direct mapping between the input signal x and the model output signal y. The memory polynomial (MP, Fig. 2(b)) and the envelope memory polynomial (EMP, Fig. 2(c)) are nonlinear models that take account of both nonlinearity orders and memory effects. The parallel twin boxes polynomial predistorter (PTB, Fig. 2(d)) is built by associating in parallel a memoryless structure and a MP structure.

3.1. Memoryless polynomial predistorter (STATIC)

Memoryless systems are very commonly modeled by Look-up-Table (LUT) mappings. We, however, focus on the alternative polynomial modeling approach thanks to its straightforward least square identification process and the lower parametric complexity that it yields. At discrete time k, distortion input–output relation is defined as

$$y[k] = H_{ST}\{x[k]\} = G(|x[k]|)e^{(j\phi_{x[k]} + \Delta_{AM/PM}(|x[k]|))}. \tag{1a}$$

where $|x[k]|$ and $\phi_{x[k]}$ denote input electrical magnitude and phase, respectively. $G(.)$ and $\Delta_{AM/PM}(.)$ are two polynomials of $|x[k]|$ of N_1 and N_2 order; they are respectively described by $\mathbf{a} = [a_0 \ldots a_{N_1}]^T$ and $\mathbf{b} = [b_0 \ldots b_{N_2}]^T$ vectors. SOA amplitude–amplitude distortions are compensated by predistortion gain $G(.)$ while SOA amplitude–phase impairments are compensated by phase shift $\Delta_{AM/PM}(.)$:

$$G(|x[k]|) = \sum_{i=0}^{N_1} a_i |x[k]|^i \text{ and } \Delta_{AM/PM}(|x[k]|) = \sum_{i=0}^{N_2} b_i |x[k]|^i \tag{1b}$$

The total number of parameters describing the model is $N_1 + N_2 + 2$.

3.2. Memory polynomial (MP) and envelope memory polynomial (EMP) predistorters

The MP predistorter, H_{MP}, is defined as a memory polynomial model of N_3 order and M_1 samples of memory as follows

$$y[k] = H_{MP}\{x\} = \sum_{i=1}^{N_3} \sum_{j=0}^{M_1-1} c_{i,j} x[k-j] |x[k-j]|^{i-1}; \ i \ odd. \tag{2a}$$

A total of $\lfloor \frac{N_3}{2} \rfloor \times M_1$ parameters is describing the model as only odd orders are actually useful.

H_{EMP} predistorter is a simplified version of the MP predistorter where only the current baseband complex input sample is taken into account:

$$y[k] = H_{EMP}\{x\} = x[k] \sum_{i=1}^{N_3} \sum_{j=0}^{M_1-1} c_{i,j} |x[k-j]|^{i-1}; \ i \ odd \tag{2b}$$

Studied MP, EMP predistorters in the following sections will be free of even nonlinearity orders.

3.3. Parallel two boxes digital polynomial predistorter (PTB)

Finally, the PTB is built on by associating in parallel (Fig. 2(d)) the memoryless polynomial structure (H_{ST}) and the MP structure (H_{MP}). For a discrete input signal $x[k]$, the predistorter output $y[k]$ is given by

$$y[k] = H_{PTB}\{x\} = H_{ST}\{x\} + H_{MP}\{x\} \tag{3a}$$

$$y[k] = \sum_{i=0}^{N_1} a_i |x[k]|^i e^{(j\phi_x + \sum_{i=0}^{N_2} b_i |x[k]|^i)}$$

$$+ \sum_{i=1}^{N_4} \sum_{j=0}^{M_2-1} d_{i,j} x[k-j] |x[k-j]|^{i-1}; \ i \ odd \tag{3b}$$

The parametric complexity amounts to $N_1 + N_2 + 2 + \lfloor \frac{N_4}{2} \rfloor \times M_2$.

4. Identification of blackbox models

Identification consists in the computation of the considered model coefficients. As predistortion is carried out in electrical domain, identification stimuli are the transmitted electrical signal x, just before E/O conversion and the received electrical signal x_r, just after O/E conversion (Fig. 1). Accordingly, a simulation with a 2^{15} 4-QAM symbols input sequence is first performed without predistortion in the transmission chain. Then x and x_r signals retrieved from simulation results are forwarded to least squares (LS) based algorithms for each predistorter set of coefficients computation.

4.1. Constrained static predistorter identification

Static parameters can be computed by applying a second order polynomial fit on the inverse AM/AM curve (Fig. 3(a)). Nevertheless directly applying this method does not always guarantee optimal polynomial coefficients regarding to Error Vector Magnitude (EVM) performance. In fact digital predistortion while compensating, to a certain amount, SOA nonlinearities tends to accentuate impairments resulting from high PAPR; the technique's overall efficiency is hence impacted. To increase EVM performance, the polynomial fitting is enforced to meet a specific constraint point $C(x_c, y_c)$ towards large amplitudes. The constraint abscissa x_c is based on the signal complementary cumulative distribution function (CCDF) of PAPR; here we consider a value on par with a 12 dB hard-clipping. The best ordinate y_c^* is then computed via a golden section search algorithm [35] within an initial interval $[0, y_c^i]$, with $y_c^i < x_c$. As can be seen in Fig. 3(b), EVM actually presents a convex variation with respect to y_c. In Table 2 default ordinate value y_0, i.e without constraints, and optimal ordinate y_c^* are compared for $x_c = 2$. It can be clearly observed that y_c^* is decreasing when the reference input power P_{ref} used for identification increases, thus achieving a crest factor reduction with no need of a separate PAPR reduction block. As a result the constrained model is showing better performance than the default static model, especially when the SOA operates in the saturated regime. An improvement of 3% can be noticed at $P_{ref} = -11$ dBm while there is practically no improvement when operating close to the SOA linear region ($P_{ref} = -18$ dBm).

In Fig. 3(c) and (d), for $P_{ref} = -14$ dBm and $P_{ref} = -11$ dBm as respective identification reference, we compare constrained and unconstrained model when input optical power P_{in} is variating from -27 dBm to -10 dBm. It is observed that the constrained inverse model is offering superior performance all over the power range. Also, as for following PTB predistorters, built up by associating a pure static block and a dynamic block, a constrained memoryless block will be chosen over a classic unconstrained static block. Parallel-Two-Boxes predistortion is presenting higher EVM improvement with optimized static component.
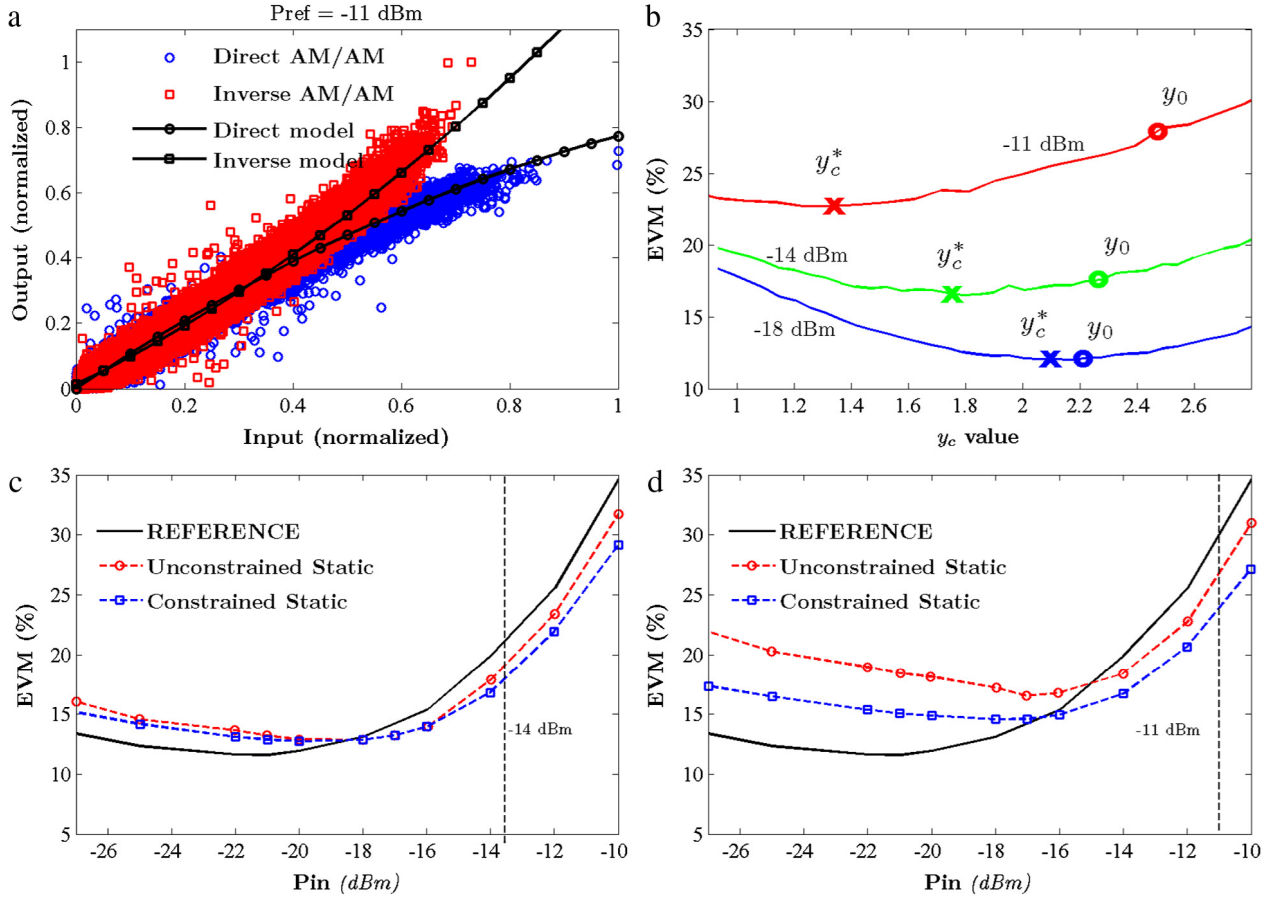
Fig. 3. (a) AM/AM direct and inverse plot, (b) EVM vs. y_c for $P_{ref} = -18, -14, -11$ dBm, (c) STATIC predistortion EVM against input power at $P_{ref} = -14$ dBm, (d) STATIC predistortion EVM against input power at $P_{ref} = -11$ dBm.

Table 2
Default ordinate y_0 vs. optimal y_c^* when constrained polynomial fitting is applied; Equivalent PAPR and EVM improvement.

P_{ref}	-18 dBm	-14 dBm	-11 dBm
Unconstrained ordinate y_0	2.2	2.26	2.41
Optimal ordinate y_c^*	2.1	1.75	1.62
Reference PAPR (dB)	8.87	8.87	8.87
STATIC predistortion PAPR (dB)	9.27	7.8	7.23
ΔEVM (%)	0.01	1.1	3

Table 3
Predistortion EVM improvement for different optical input levels at $P_{ref} = -14$ dBm.

P_{in}	-26 dBm	-20 dBm	-14 dBm	-11 dBm	Complexity
STATIC	-1.8	-0.72	**3.18**	4.45	6
MP	-2.84	-0.32	**4.57**	3.78	15
EMP	-5.72	-2.6	**6.3**	6.86	15
PTB	0.56	2.34	**5.84**	6.36	12

4.2. Memory polynomial predistorters identification

Although they implement nonlinear functions, MP predistorters have a linear input–output relation with respect to model parameters. MP, EMP and PTB will accordingly be identified by an offline LS algorithm which relies on a QR decomposition for better numerical stability [36]. Identification stimuli are the same 2^{15} 4-QAM x and x_r signals used to compute static model parameters. Identification is carried out for $P_{ref} = -18, -14$ and -11 dBm.

4.2.1. Parametric complexity sweep

Model order and memory depth settings are not known a priori. We therefore proceed to the identification of a series of predistorters with different order and memory depth configuration. Order and depth are varying from 1 to 5, only odd orders being used. Each predistorter is identified and related validation simulations are carried out. In Fig. 4 EVM against optical input power P_{in} is presented. Results are first shown for $P_{ref} = -14$ dBm.

▶ In Fig. 4(a), it is seen that a MP parametric complexity of ($N_3 = 3$ and $M_1 = 5$) provides the best performance at a limited parametric

complexity (10 coefficients). One should remember that the main region of interest concerns high power values where the SOA operates close to the identification power ($P_{ref} = -14$ dBm). Hence when $P_{in} < -20$ dBm, only linear predistorters are providing a gain in EVM.

▶ In Fig. 4(b), EMP plots are similar to MP ones. A third order EMP predistorter with a memory depth of 5 provides the best results when P_{in} is close to the identification optical power $P_{ref} = 14$ dBm. When the operating point is moving towards the linear region ($P_{in} < -18$ dBm) it can be observed that all the predistorters are degrading the CO-OFDM transmitter performance.

▶ In Fig. 4(c) PTB predistorters present performances comparable to MP ones when the component exhibits nonlinear effects (order > 1). However best results are obtained when the dynamics is linear. It is hence seen that the two-box structure with a constrained static bloc and linear dynamic (FIR) is providing improvement for a wide range of optical input powers and is therefore more robust to P_{in} variations.

The overall performance of STATIC, MP, EMP and PTB predistortion are compared in Fig. 4(d) and Table 3. EMP predistortion presents the best EVM gain at high power, slightly better than PTB predistortion. EMP predistortion is however not very robust to decreasing P_{in} values contrary to PTB predistortion which is providing improvement for input power as low as $P_{in} = -26$ dBm. As for the two other predistorters they
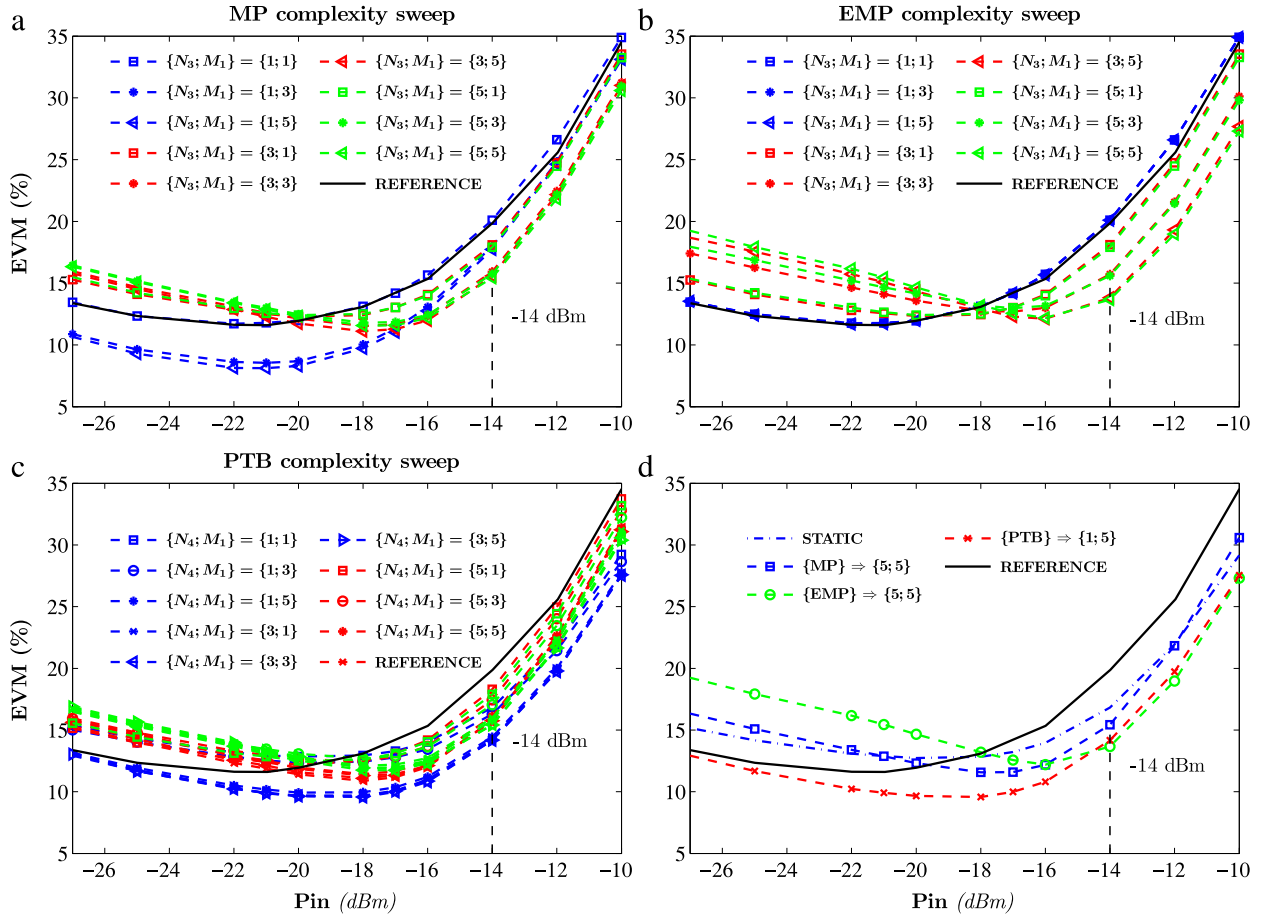
Fig. 4. Predistortion parametric complexity sweep for an identification power at $P_{ref} = -14$ dBm, (a) MP, (b) EMP, (c) PTB and (d) comparison plot.

are inferior in performance. MP predistortion is however more efficient than constrained STATIC predistortion for P_{in} ranging from -22 dBm to -12 dBm.

4.2.2. Optical input power influence

The previous results are relative to an identification at $P_{ref} = -14$ dBm. We now present validation results for $P_{ref} = -18$ dBm (low power) and $P_{ref} = -11$ dBm (high power). Orders and memory depth are kept the same. Predistortion performance is compared in Fig. 5 and Table 3. The basic trend is that increasing identification input power (P_{ref}) will allow for more predistortion gain in high power and degraded EVM in low power.

▶ For $P_{ref} = -18$ dBm, close to the linear regime of the SOA (Fig. 5(a)), MP and PTB predistortion have very similar behavior. EMP presents the same performance in high power and a poor performance in low power. The less efficient structure is the STATIC predistorter.

▶ For $P_{ref} = -11$ dBm, in a very saturated operating point (Fig. 5(b)), as for $P_{in} = -14$ dBm, EMP and PTB predistorters have close performance in high power. However EMP scheme is very sensitive to the decrease in P_{in}. For instance at $P_{in} = -16$ dBm, EMP predistortion induces a loss in EVM of 3% while PTB predistortion still provides an EVM gain of 2%. MP predistortion is very inefficient, having a performance inferior to the STATIC predistortion all over presented optical input power range.

In Fig. 5(c) and Fig. 5(d) PAPR is evaluated at the output of various predistorters, for $P_{ref} = -18$ dBm and $P_{ref} = -11$ dBm. At low power the PTB design induces the highest crest factor (11.7 dB) followed by EMP, MP and STATIC approaches with a PAPR of 9.9 dB, 9.83 dB, and 9.27 dB, respectively, while the original OFDM signal

exhibits a PAPR of 8.87 dB. For $P_{ref} = -11$ dBm multiple remarks can be derived. STATIC predistortion actually induces a PAPR reduction. While reference electrical OFDM PAPR is unchanged (8.87 dB), the static predistorter leads to a PAPR of 7.23 dB. In fact due to the high power identification level, the non-constrained memoryless predistorter is less efficient (Fig. 3(b)). Constrained static identification is yielding optimal coefficients that induces a PAPR reduction. It has also to be noted that MP and EMP predistortion are very sensitive to saturated operating point identification. They respectively present 11.97 and 11.67 dB of PAPR while PTB PAPR is at 11.97 dB. However high order polynomial predistorters identified at a very saturated operating point induce low performance when operating at a input power far inferior to the identification reference (i.e $P_{ref} = -11$ dBm). Impairments' precompensation is provided when the SOA exhibits linear behavior. Comparatively, the PTB design which is providing good performance without the need of high polynomial orders has a significant better performance at low power.

4.2.3. BER performance

The EVM criterion has the advantage that it can be easily evaluated whatever the operating point is, but the Bit Error Rate (BER) is more representative of the system performance from a practical point of view. Estimating the BER from the EVM in presence of strong nonlinear effects may lead to erroneous conclusions, so we conducted Monte Carlo simulations so as to evaluate the BER. Due to the relatively low EVM observed over the whole operating range, a large computational burden has been required for this evaluation. For this reason we considered only the case where the predistorters are identified at $P_{ref} = -11$ dBm, yielding EVM values above 20%. The results are depicted in Fig. 6. It can
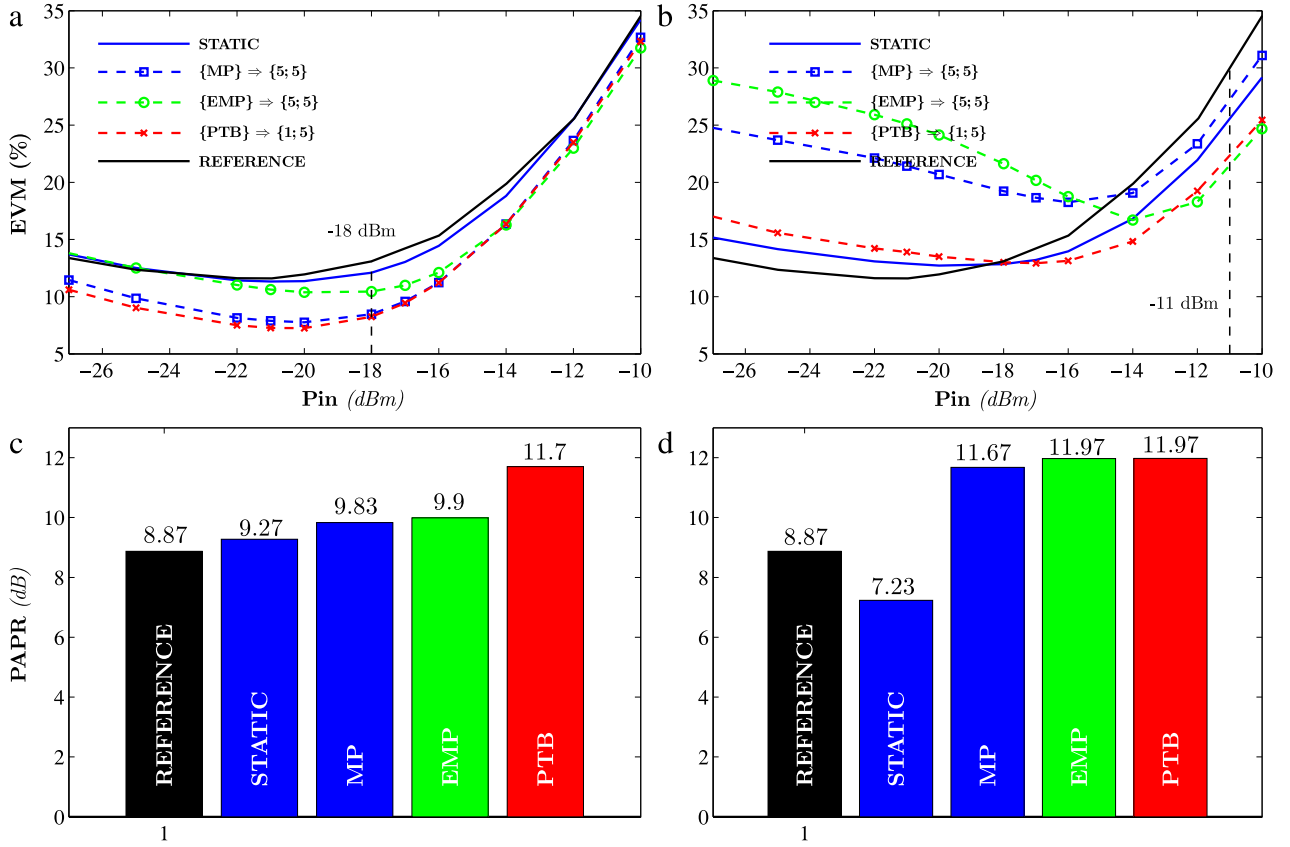
Fig. 5. Predistortion performance at (a) $P_{ref} = -18$ dBm, (b) $P_{ref} = -11$ dBm and Predistortion PAPR (c) $P_{ref} = -18$ dBm and (d) $P_{ref} = -11$ dBm.
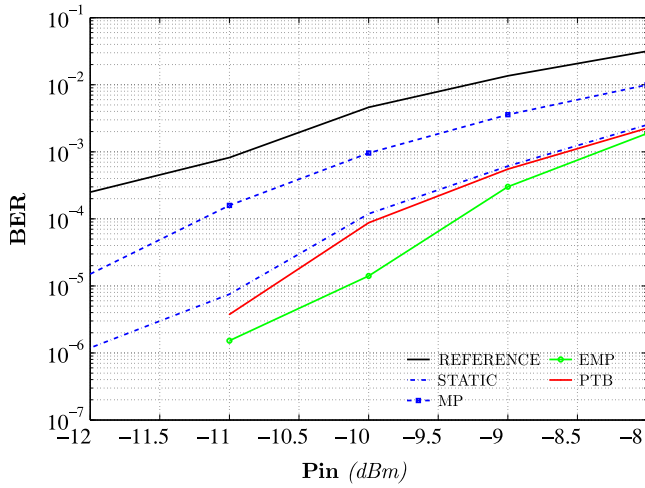

Fig. 6. BER against SOA input power for an identification at $P_{ref} = -11$ dBm.

be seen that the EMP design offers the best performance in the vicinity of P_{ref}, with a clear advantage over the PTB design, but keeping in mind that a crossing between the BER curves should occur around -12 dBm (which does not appear on the plot due to the difficulty to evaluate BERs of the order of 10^{-6}). The sensitivity of the EMP predistorter to optical power, with respect to P_{ref} can be seen at $P_{in} = -8$ dBm where a close performance is obtained for the PTB and EMP designs. Another observation is that the proposed Static design offers a close BER performance to the PTB when operating at high power, as a result of PAPR reduction.

4.2.4. DAC/ADC resolution influence

The 12 bits resolution considered so far for the DAC/ADC may not be realistic in many practical applications. We subsequently examine the influence of an increased quantization step using 4 bits, which translates into a significant change in signal dynamics and may lead to a different behavior for the considered predistorters. We focus on the case of an identification at -11 dBm, where the nonlinear effects are the more significant, and keeping the same values as before for the predistorters order and memory length. The results are depicted in Fig. 7. Again, the MP scheme appears to be the less effective approach, with very few EVM improvement at P_{ref} and a high sensitivity to optical power variation. The EMP predistorter offers the better performance in the vicinity of the reference power, with a slightly more pronounced advantage over the PTB scheme, but once again the EMP method is not robust when the operating point deviates from the identification point. It can be seen that the PTB technique gives the best tradeoff as previously observed for a finer DAC/ADC resolution. The constrained static design could also be considered as a pertinent tradeoff if a very low complexity is targeted.

5. Robustness analysis

Robustness analysis is presented throughout this section. The analysis will focus on five different cases. First we will study robustness with respect to IQ modulator peak-to-peak Voltage (V_{pp}). Then SOA biasing current (I_{bias}) and laser wavelength (λ) variation impact are evaluated. The impact of the number of subcarriers on predistortion performance is also assessed. Finally the default SOA INPHENIX-IPSAD1501 model is tweaked, through its Henry factor (α_H) to exhibit a more pronounced nonlinear behavior. Predistortion performance is then studied in this configuration. By default, validation simulations are performed with 2^{13} 4-QAM symbols while models were identified with 2^{15} 4-QAM symbols.
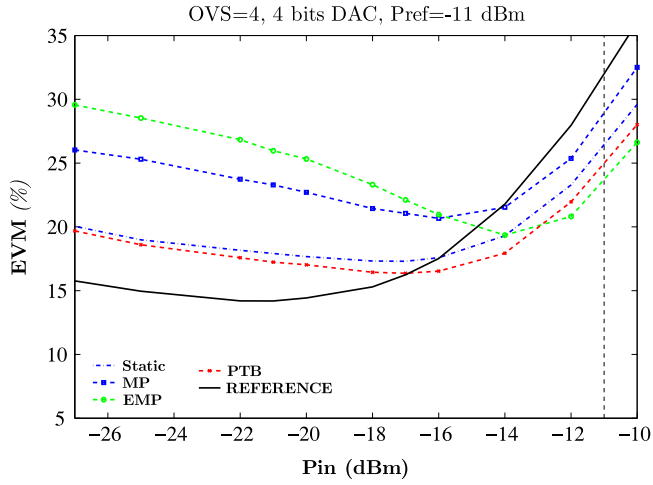
Fig. 7. Predistortion performance with a DAC/ADC resolution of 4 bits, for an identification at $P_{ref} = -11$ dBm.

5.1. IQ modulator voltage sweep

Robustness against IQ modulator Peak-to-Peak Voltage (V_{pp}) will be studied for two different test cases: At low power where the SOA exhibits a quasi-linear behavior and at high power where the device is operating in saturation mode. We proceed as follows; default V_{pp} voltage

is first set at 8 Volts, the voltage used so far. Then optical attenuation is determined to meet two input power settings: −21 dBm (low power case) and −13 dBm (high power case). Once determined, attenuation values are left unchanged. Robustness analysis will then consist in sweeping V_{pp} from 1 Volts to 15 Volts and in assessing EVM evolution. In Fig. 8(a), input power P_{in} against V_{pp} is plotted. A nonlinear dependence is observed. In Fig. 8(b), EVM against V_{pp} is presented for the first test case (−21 dBm initial setting). For decreasing V_{pp} values under 3 Volts, EVM is rapidly growing up due to low optical input power ($P_{in} \approx$ −35 dBm) and a significant impact of ASE noise on the transmission quality (low OSNR). For high V_{pp} values, as SOA is operating close to its saturation point, EVM is also increasing due to nonlinear impairments, the rate is however slower. In Fig. 8(b), identified STATIC, MP, EMP and PTB predisorters are improving system performance when $V_{pp} > 3$ V corresponding to $P_{in} = -31$ dBm. MP and PTB predistortion offer the best EVM improvement and have close behaviors. For V_{pp} close to 14 Volts, up to 5% of EVM gain is obtained. A value which is consistent with EVM improvement for optical input power P_{in} close to −20 dBm (Fig. 5(a) and Fig. 8(a)). In fact controlling V_{pp} is an indirect way for setting input optical power P_{in} as shown in Fig. 8(a). EVM against V_{pp} is thus directly related to EVM against input power, P_{in} being either set through an attenuator or indirectly through V_{pp}. This is verified with the second test case. For this test case ASE effect (low V_{pp} values) and saturation impairments (high V_{pp} values) are still present leading to EVM loss. Saturation impairments are however more pronounced and EVM is rapidly increasing for high V_{pp} values. This is due to the initial −13 dBm power setting. For the very saturated region (high V_{pp}) EMP predistortion is providing the best improvement up to 11.6% for
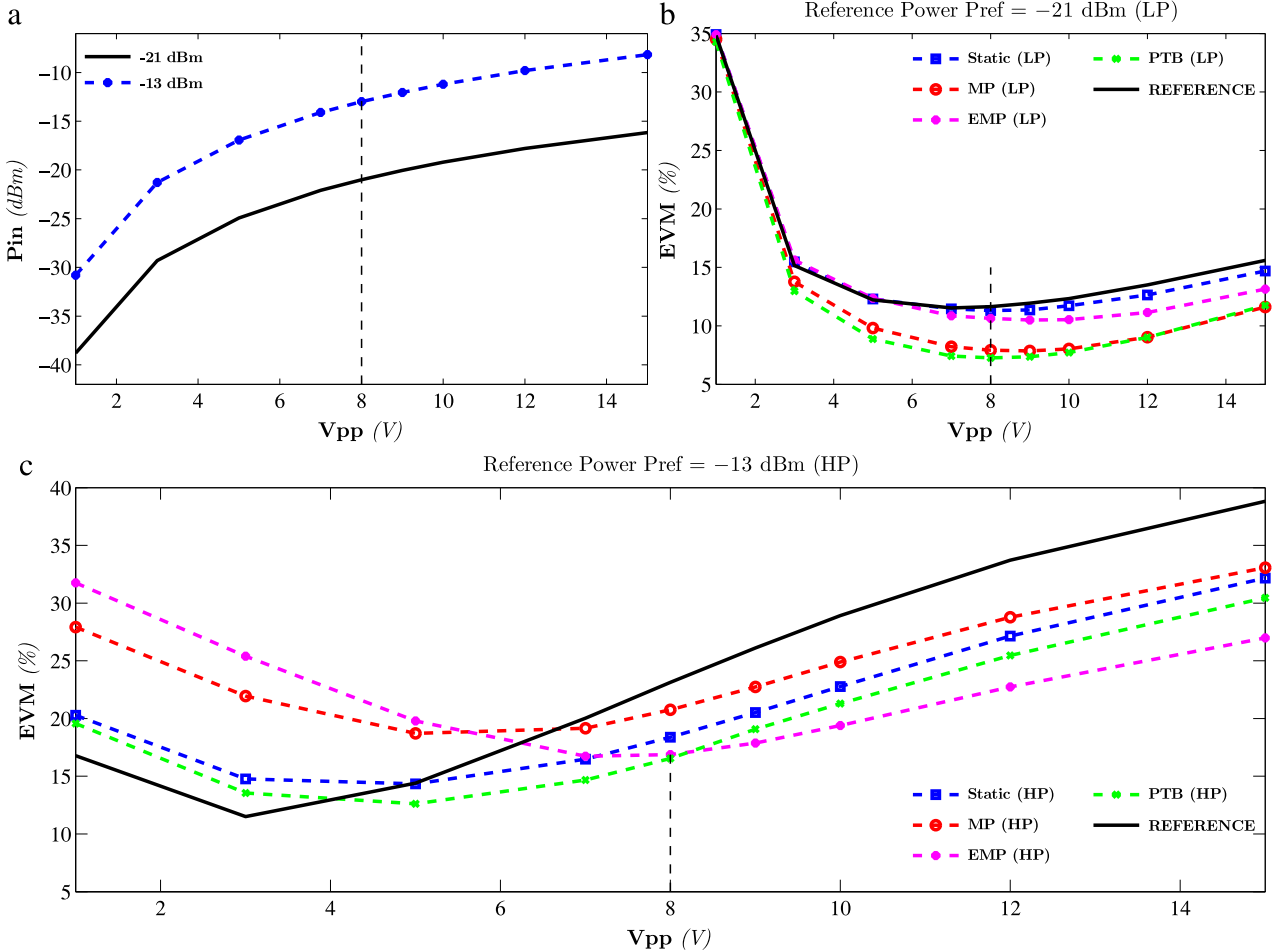

Fig. 8. (a) Input optical power against Peak-to-Peak Voltage, (b) EVM against Peak-to-Peak Voltage for a −21 dBm input power, (c) EVM against Peak-to-Peak Voltage for a −13 dBm input power.

Table 4
Predistortion EVM improvement for different values of peak-to-peak voltage.

V_{pp} (Volts)	2	6	10	14
P_{in} (dBm)	−26.05	−16	−11.21	−8.52
STATIC	−3.38	1.8	6.14	6.67
MP	−10.79	−1.74	4.04	5.52
EMP	−14.44	−1	9.51	11.6
PTB	−2.41	3.57	7.61	8.4

V_{pp} = 14 Volts corresponding to P_{in} close to −8.5 dBm. It is followed by PTB predistortion (8.4%), constrained static predistortion (6.67%), and finally MP (5.52%) (Fig. 8(c) and Table 4). For V_{pp} = 2 Volts and $P_{in} \approx -26$ dBm PTB (−2.41%) and Static (−3.38%) predistortion present less EVM degradation. As it could be expected referring to Fig. 5(b). EMP is presenting the worst performance with an EVM loss of −14.44% (Table 4).

5.2. Biasing current influence

So far simulations were carried out for a fixed 150 mA injection current (I_{bias}) setting. We now proceed to biasing current sweep from 117 to 220 mA. Two initial power levels are considered, −21 dBm (low power case) and −13 dBm (high power case). As presented in Fig. 9(a), the direct effect of injection current variation is a change in SOA gain. In Fig. 9(a) gain evolution with respect to both input power (P_{in}) and bias current (I_{bias}) is plotted. SOA gain is increasing with the biasing current. In Fig. 9(b) we also observe that higher biasing current results in degraded EVM performance. We compared predistortion performance for two reference levels, −21 and −13 dBm. At −21 dBm reference

EVM (11.6%) and predistortion EVM is quasi-constant (less than 1% variation) with respect to biasing current over the range [120,220] mA. In this case PTB is providing the best performance followed by MP, EMP and static predistorters, with an EVM improvement of 4.6%, 4%, 2%, 0.5%, respectively. At −13 dBm (Fig. 9(c) and Table 5), EMP predistortion is providing best performance at high power and the worst at low power; EVM improvement is up to 11.13% at 220 mA. PTB, STATIC and MP EVM gains are respectively at 9.17%, 7.39% and 4.74% for the same biasing current value. One should also notice that for the reference I_{bias} = 150 mA, PTB and EMP have equivalent performance (17% of EVM). EMP is providing up to 2% superior performance at I_{bias} = 220 mA. In Fig. 9(d), we plotted EVM against output power P_{out} instead of P_{in} or I_{bias}. A higher output power is providing a longer transmission reach. We are now comparing EVM against P_{out} variations, first by controlling optical attenuation just before the SOA and then through directly increasing I_{bias}. EVM against P_{out} without predistortion and with EMP predistortion is plotted for both approaches. It can be clearly observed that a better predistortion performance may be achieved if the reach is extended by increasing the bias current. For instance at a given optical output power P_{out} = 4.5 dBm and a 220 mA I_{bias} setting, EMP predistortion is providing up to 14% of EVM improvement; while for the same output power and a bias current lowered at 150 mA EMP improvement decreases to 11%.

5.3. Wavelength shift influence

We also study robustness with respect to laser wavelength λ which is swept from 1500 to 1560 nm (reference at 1540 nm). SOA gain evolution is presented in Fig. 10(a), attaining a peak around 1520 nm. EVM against P_{in} curves for different wavelengths are then plotted in
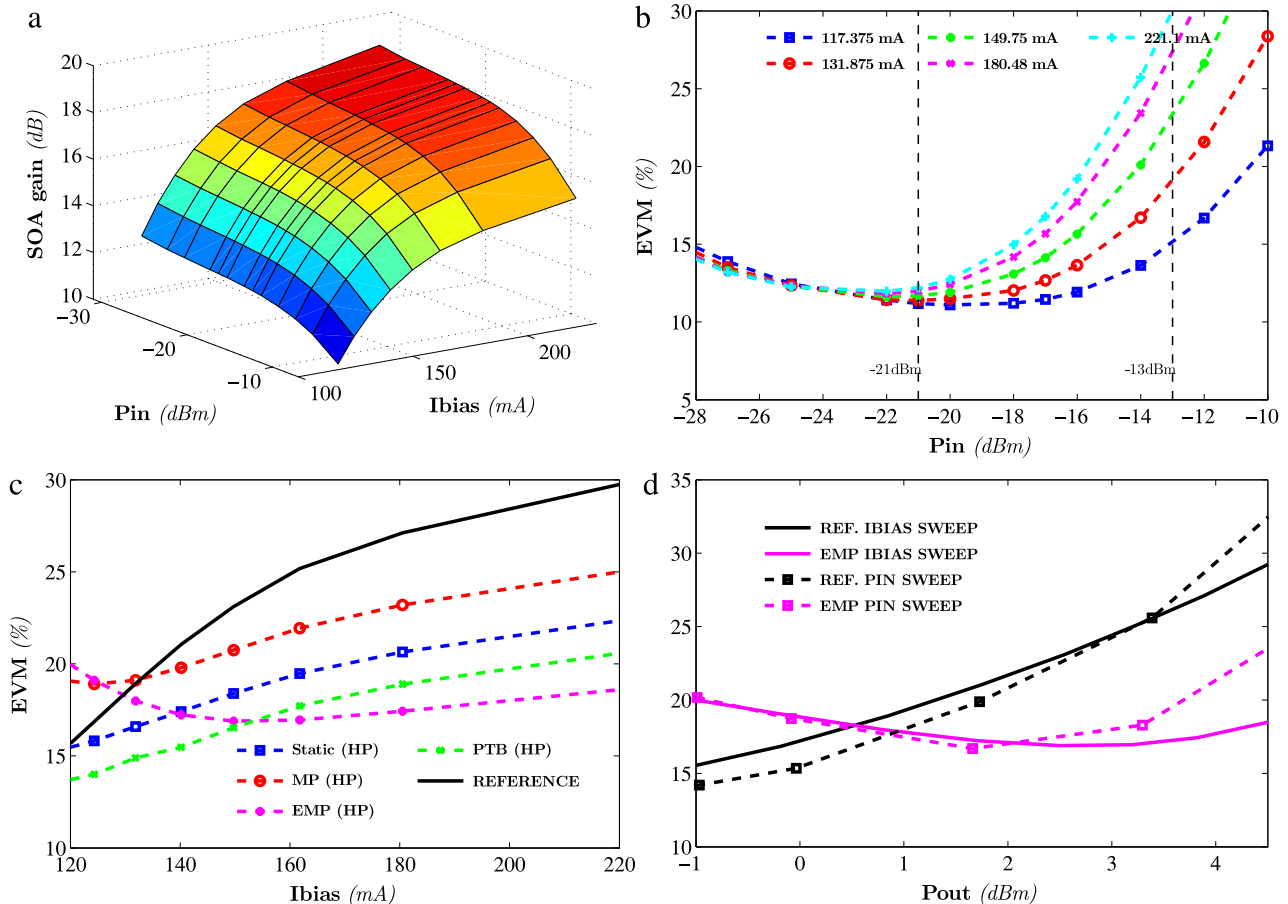

Fig. 9. (a) SOA gain with respect to injected power and biasing current static variations, (b) EVM against injected power for different biasing current values (c) EVM against biasing current at a fixed P_{ref} at −13 dBm, (d) EVM against Output power by varying input power directly through attenuation or via biasing current.
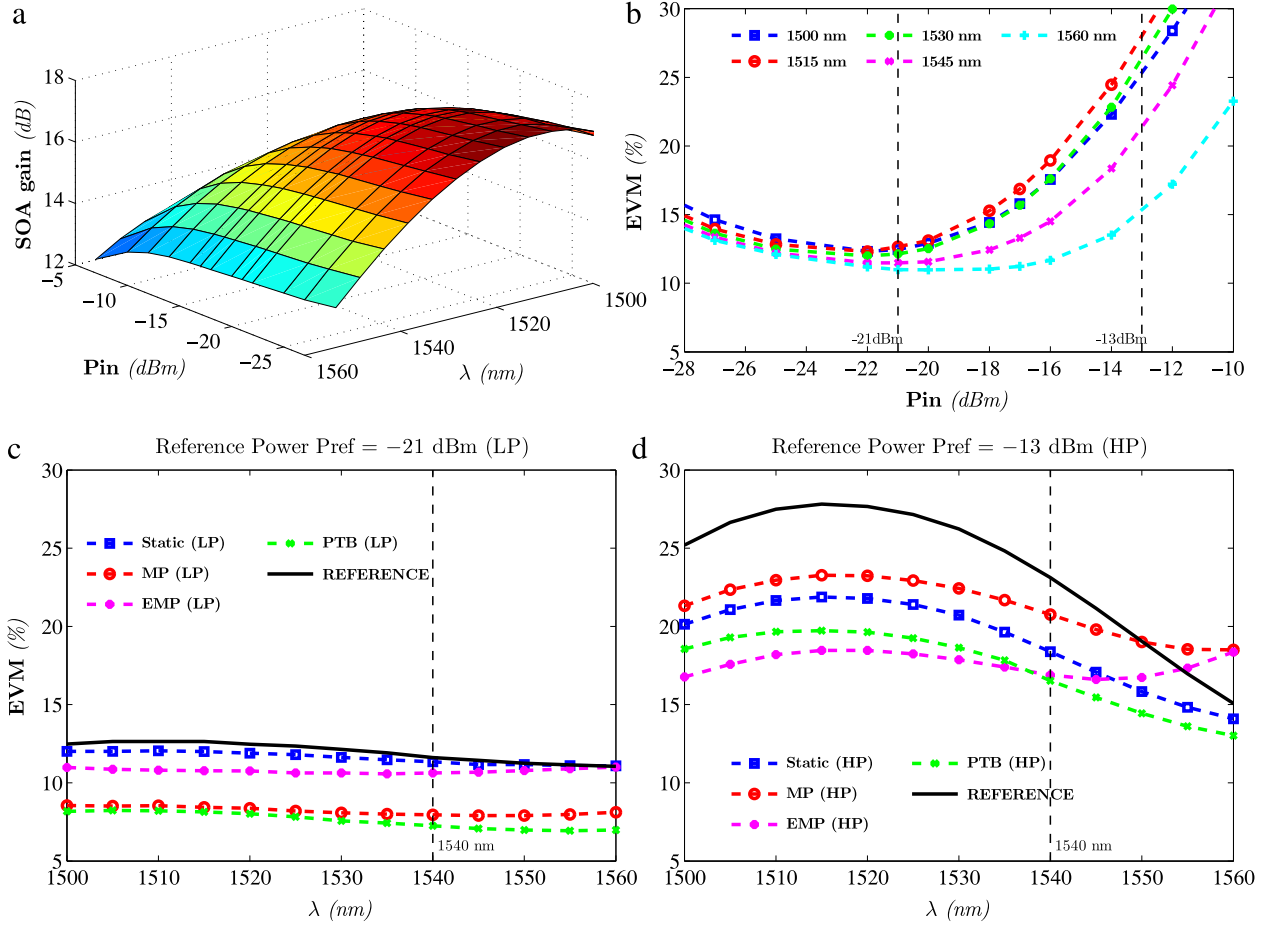
Fig. 10. (a) SOA gain with respect to injected power and input wavelength variations, (b) EVM against injected power for different input wavelengths (c) EVM against input wavelength at a fixed P_{in} at −21 dBm, (d) EVM against input wavelength at a fixed P_{in} at −13 dBm.

Table 5
Predistortion EVM improvement for varying biasing current.

Biasing current (mA)	120	160	200	220
STATIC	0.11	5.56	6.9	7.39
MP	−3.5	3.12	4.31	4.74
EMP	−4.53	7.94	10.38	11.13
PTB	1.86	7.33	8.66	9.17

Table 6
Predistortion EVM improvement for varying input wavelength; $P_{ref} = -13$ dBm.

λ (nm)	1500	1520	1540	1560
STATIC	4.87	5.88	4.73	0.98
MP	3.68	4.43	2.34	−3.43
EMP	8.23	9.21	6.61	−3.29
PTB	6.44	8.04	6.24	2.06

Fig. 10(b). At −21 dBm, reference EVM is close to 12% and is stable with respect to λ variations. PTB and MP predistorters are offering the highest performance around 5% of stable EVM improvement for each predistorter. At higher power (−13 dBm), EMP predistortion offers the best performance for $\lambda < 1540$ nm. For $\lambda = 1520$ nm (Table 6), an improvement of 9.21% is observed for the EMP predistorter; PTB, STATIC and MP designs offer an improvement of 8.04%, 5.88% and 4.43%, respectively. As the SOA operates close to its saturation gain at 1520 nm, impairments are more pronounced and EMP offers the best performance. It is also noticed that when λ is close to 1560 nm, EMP and MP predistorters perform worst, inducing respectively an EVM loss of −3.29% and −3.43%. This is due to the device's lower gain. The SOA is getting close to a linear operating point and (EMP, MP) identified at $P_{ref} = -11$ dBm are less efficient. The PTB still provides a 2.06% EVM improvement while constrained static predistortion offers providing around 1% of improvement.

5.4. Number of subcarriers sweep

We now consider a varying number of subcarriers (N_{sc}) from 64 to 2048. To be consistent with the digital predistorter's sampling period

we accordingly sweep symbol time T_u from 12.8 to 409.6 ns (initial $T_u = 25.6$ ns is taken as reference). Bandwidth is thus constant. Simulations are now carried out with a sequence of 2^{15} 4-QAM symbols. Results are shown in (Fig. 11) for low (−21 dBm) and high power (−13 dBm). We observe, for both cases, a slight deviation in EVM when number of subcarriers is varying (Fig. 11(a) and (b)). As presented in previous paragraphs, predistortion is more sensitive to P_{out} variations either via P_{in}, V_{pp}, biasing current or input wavelength λ particularly for saturation point identification. We rather observe a robust behavior with respect to N_{sc} variation either at low or high power.

5.5. Influence of phase–amplitude coupling

We assess predistortion performance and robustness in the case of a SOA exhibiting much stronger phase–amplitude coupling. To that end SOA Henry factor α_H which was previously set at 3.3 is now set at 5. A new identification has been carried out for static, EMP and PTB predistortion with $P_{ref} = -14$ dBm. MP predistortion providing lower performance in case of strong nonlinearities is not presented. In Fig. 12(a) the general plot representing EVM with respect to input power P_{in} and α_H is shown. Greater EVM values are obtained when α_H
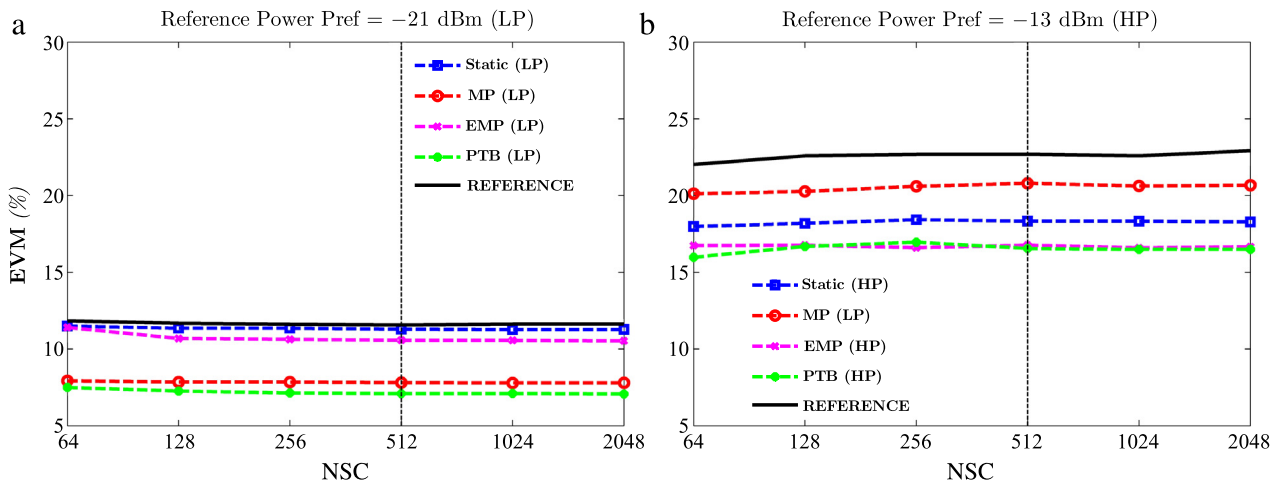
Fig. 11. (a) EVM against number of subcarriers at $P_{in} = -21$ dBm, (b) EVM against number of subcarriers at $P_{in} = -13$ dBm.
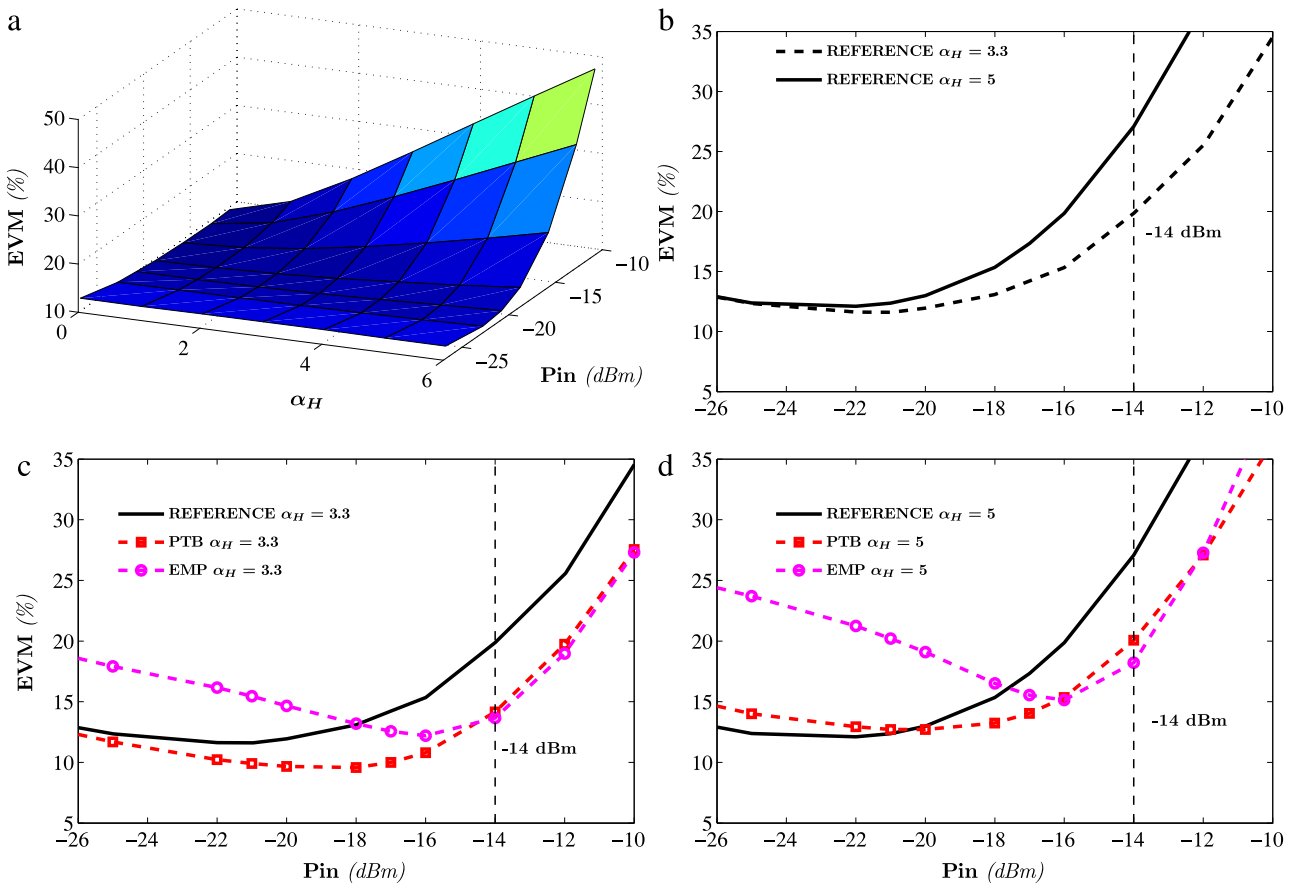

Fig. 12. (a) EVM against injected power and Henry factor, (b) EVM against injected power for $\alpha_H = 3.3$ and $\alpha_H = 3.3$, (c) predistortion EVM performance for $\alpha_H = 3.3$, (d) predistortion EVM performance for $\alpha_H = 5$.

is increasing. In Fig. 12(b) a comparison of EVM against input power, for the two distinct values of the Henry factor, is also plotted. In Table 7 we compare the second order static predistorter optimal ordinate y_c^* for the two values of Henry factor. As increasing α_H generates higher nonlinearities the optimal ordinate y_c^* is decreasing (see paragraph 4.1).

Then EMP predistortion and PTB predistortion are compared in Fig. 12(c) and Table 8 for $\alpha_H = 3.3$ and $\alpha_H = 5$ at $P_{ref} = -14$ dBm. EMP and PTB predistortion present a close improvement at high power; for $P_{in} = -12$ dBm they respectively offer an improvement of 5.86% and 6.62% in EVM. In the case of $\alpha_H = 5$, EMP and PTB predistortion are

Table 7
Optimal constrained static predistorter ordinate y_c^* for $\alpha_H = 3.3$ and $\alpha_H = 5$.

P_{ref}	−18 dBm	−14 dBm	−11 dBm
$\alpha_H = 3.3$	2.1	1.75	1.62
$\alpha_H = 5$	1.94	1.36	1.01

respectively providing 9.71% and 9.89% in EVM improvement for the same input level. Still for $P_{in} = -12$ dBm, reference EVM is at 25% and 35% respectively for $\alpha_H = 3.3$ and $\alpha_H = 5$.

Table 8

EMP and PTB predistortion EVM improvement for $\alpha_H = 3.3$ and $\alpha_H = 5$ at $P_{ref} = -14$ dBm.

P_{in} (dBm)	−25	−20	−16	−12
EMP, $\alpha_H = 5$	−11.31	−6.1	4.72	9.71
PTB, $\alpha_H = 5$	−1.63	0.27	4.45	9.89
EMP, $\alpha_H = 3.3$	−5.57	−2.7	3.15	6.62
PTB, $\alpha_H = 3.3$	0.66	2.28	4.54	5.86

6. Conclusion

Various digital baseband predistorters have been investigated in this paper for improving the EVM performance of an SOA-based 17 Gbps CO-OFDM transmitter, while considering the criterion of robustness against system parametric variations. A special focus is given to a parallel two-box (PTB) behavioral model, combining a static nonlinear function with a memory polynomial (MP) model. A simple design of the static function has been first proposed for jointly achieving linearization and reduction of the peak amplitudes. Then, the study of the parametric complexity of the different predistorters (STATIC, MP, EMP, PTB) revealed that the PTB scheme with constrained static and linear dynamics (FIR) is providing the best performance, with an EVM improvement over a wide range of optical input power with a single identification at −14 dBm. Furthermore, it is shown that predistortion robustness against optical input power variation is strongly dependent on the operating point chosen for identification. Generally speaking, the polynomial predistorters studied throughout the paper are sensitive to output optical power fluctuations, either directly, or through parameters such as IQ modulator peak-to-peak voltage, SOA biasing current or even input wavelength. Overall, the PTB structure offers the best compromise. It is a low-complexity design capable of lowering EVM over a wide range of transmitter parameter values.

References

[1] W. Shieh, I.B. Djordjevic, OFDM for Optical Communications, Elsevier/Academic Press, 2009.

[2] A.J. Lowery, L.B. Du, Optical orthogonal division multiplexing for long haul optical communications: A review of the first five years, Opt. Fiber Technol., Mater. Devices Syst. 17 (2011) 421–438.

[3] N. Cvijetic, OFDM for next-generation optical access networks, J. Lightwave Technol. 30 (4) (2012) 384–398.

[4] H. Ochiai, H. Imai, On the distribution of the peak-to-average power ratio in OFDM signals, IEEE Trans. Commun. 49 (2) (2001) 282–289.

[5] Y. Rahmatallah, S. Mohan, Peak-to-average power ratio reduction in OFDM systems: A survey and taxonomy, IEEE Commun. Surv. Tutor. 15 (4) (2013) 1567–1592.

[6] B. Goebel, S. Hellerbrand, N. Haufe, N. Hanik, PAPR reduction techniques for coherent optical OFDM transmission, in: Proc. IEEE Int. Conf. on Transparent Optical Networks (ICTON) 2009, Azores, Portugal, Jul. 2009.

[7] S. Amiralizadeh, A.T. Nguyen, L.A. Rusch, Modeling and compensation of transmitter nonlinearity in coherent optical OFDM, Opt. Express 23 (20) (2015) 26192–26207.

[8] H. Khaleghi, P. Morel, A. Sharaiha, T. Rampone, Experimental validation of numerical simulations and performance analysis of a coherent optical-OFDM transmission system employing a semiconductor optical amplifier, IEEE J. Lightwave Technol. 31 (1) (2013) 161–170.

[9] S. Bejan, S. Azou, P. Morel, C. Diouf, M. Telescu, N. Tanguy, A. Sharaiha, A joint linearization/companding approach for improving a CO-OFDM transmitter, IEEE Photonics Technol. Lett. 27 (20) (2015) 2162–2165.

[10] M.J. Connelly, Semiconductor Optical Amplifiers, Kluwer, Boston, MA, 2002.

[11] H. Schmuck, et al., Demonstration of an SOA-assisted open metro-access infrastructure for heterogeneous services, Opt. Express 22 (1) (2014) 737–748.

[12] C. Tai, S.-L. Tzeng, H.-C. Chang, W.I. Way, Reduction of nonlinear distortion in mqw semiconductor optical amplifier using light injection and its application in multichannel m-qam signal transmission systems, IEEE Photonics Technol. Lett. 10 (1998) 609–611.

[13] F. Tabatabai, H.S. Al-Raweshidy, Feed-forward linearization technique for reducing non-linearity in semiconductor optical amplifier, J. Lightwave Technol. 25 (9) (2007) 2667–2674.

[14] X. Zhang, R. Zhu, D. Shen, T. Liu, Linearization technologies for broadband radio-over-fiber transmission systems, Photonics 1 (4) (2014) 455–472.

[15] F.M. Ghannouchi, O. Hammi, M. Helaoui, Behavioral Modeling and Predistortion of Wireless Transmitters, Wiley, New York, 2015.

[16] L. Guan, A. Zhu, Green communications: Digital predistortion for wideband RF power amplifiers, IEEE Microwave Mag. (2014).

[17] A. Hekkala, M. Lasanen, L.C. Vieira, N.J. Gomes, A. Nkansah, Architectures for joint compensation of RoF and PA with nonideal feedback, in: Vehicular Technology Conference, VTC 2010-Spring, 16–19 May 2010, Taipei, Taiwan, 2010.

[18] L.C. Vieira, N.J. Gomes, A. Nkansah, F. van Dijk, Behavioral modeling of radio-over-fiber links using memory polynomials, in: Proc. IEEE Int. Topical Meeting on Microwave Photonics, Montreal, Canada, 2010.

[19] A.V. Cartaxo, T.M. Alves, F.W. Carvalho, J.A. Morgado, Linearization techniques of electro-optical converters for multi-format OFDM-based PONs, in: 14th IEEE International Conference on Transparent Optical Networks, ICTON, Coventry, UK, 2012.

[20] A. Hekkala, M. Hiivala, M. Lasanen, J. Perttu, L.C. Vieira, N.J. Gomes, A. Nkansah, Predistortion of radio over fiber links: algorithms, implementation, and measurements, IEEE Trans. Circuits Syst.-I 59 (3) (2012) 664–672.

[21] Y. Pei, K. Xu, J. Li, A. Zhang, Y. Dai, Y. Ji, J. Lin, Complexity-reduced digital predistortion for subcarrier multiplexed radio over fiber systems transmitting sparse multi-band RF signals, Opt. Express 21 (3) (2013) 3708–3714.

[22] H. Chen, J. Li, K. Xu, Y. Pei, Y. Dai, F. Yin, J. Lin, Experimental investigation on multi-dimensional digital predistortion for multi-band radio-over-fiber systems, Opt. Express 22 (4) (2014) 4649–4661.

[23] Y. Zhang, J. Li, H. Chen, C. Yin, Y. Dai, F. Yin, K. Xu, Clip-and-filter-based crest factor reduction and digital predistortion for WLAN-over-fiber links, IEEE Photonics Technol. Lett. 26 (23) (2014) 2315–2318.

[24] F. Carvalho, A. Cartaxo, Broad baseband nonlinear distortion mitigation using digital pre-and post-distortion in OFDM-based WDM LR-PON, Opt. Express 23 (6) (2015) 7062–7074.

[25] L.C. Vieira, N.J. Gomes, Clipping and predistortion for compensation of OFDM-Radio over Fiber link distortion, in: IEEE International Conference on Communications, London, UK, 2015, pp. 977–981.

[26] G. Khanna, B. Spinnler, S. Calabr, E. De Man, N. Hanik, Robust adaptive pre-distortion method foroptical communication transmitters, IEEE Photonics Technol. Lett. 28 (7) (2016) 752–759.

[27] Z. Liu, M.A. Violas, N.B. Carvalho, Digital predistortion for RSOAs as external modulators in radio over fiber systems, Opt. Express 19 (18) (2011) 17641–17646.

[28] Y. Bao, Z. Li, J. Li, X. Feng, B.O. Guan, G. Li, Nonlinearity mitigation for high-speed optical OFDM transmitters using digital pre-distortion, Opt. Express 21 (6) (2013) 7354–7361.

[29] H. Moon, R. Sedaghat, FPGA-based adaptive digital predistortion for radio-over-fiber links, Microprocess. Microsyst. 30 (3) (2006) 145–154.

[30] X.N. Fernando, A.B. Sesay, Higher order adaptive filter based predistortion for nonlinear distortion compensation of radio over fiber links, in: IEEE International Conference on Communications, Vol. 1, New Orleans, LA, USA, pp. 367–371, 2000.

[31] L.C. Vieira, N.J. Gomes, A. Nkansah, F. van Dijk, Study of complex-envelope behavioral models for radio-over-fiber link nonlinearities. in: IEEE Global Communications Conference, GLOBECOM, Anaheim, CA, USA, Dec. 2012, pp. 3098–3103.

[32] A.K. Vyas, N. Agrawal, Development of hybrid envelop memory polynomial based predistorter for RoF system, Optik-Int. J. Light Electron Opt. 127 (11) (2016) 4768–4773.

[33] P.W. Berenguer, M. Nlle, L. Molle, T. Raman, A. Napoli, C. Schubert, J.K. Fischer, Nonlinear digital pre-distortion of transmitter components, J. Lightwave Technol. 34 (8) (2016) 1739–1745.

[34] E. Agrell, et al., Roadmap of optical communications, J. Opt. 18 (6) (2016).

[35] W.H. Press, S.A. Teukolsky, W.T. Vetterling, B.P. Flannery, Numerical Recipes: The Art of Scientific Computing, third ed., Cambridge University Press, New York, 2007.

[36] C.C. Paige, M.A. Saunders, LSQR: An algorithm for sparse linear equations and sparse least squares, ACM Trans. Math. Software 8 (1) (1982) 43–71.